Geophysical Prospecting EAGE EUROPEAN ASSOCIATION OF GEOSCIENTISTS & ENGINEERS

Geophysical Prospecting, 2013, **61**, 270–286 doi: 10.1111/1365-2478.12030

Sensitivity of flow and elastic properties to fabric heterogeneity in carbonates

Ravi Sharma[1]*, Manika Prasad[1], Mike Batzle[1] and Sandra Vega[2]

[1]*Colorado School of Mines, Golden, Colorado, USA and* [2]*Petroleum Institute, Abu Dhabi, UAE*

Received May 2012, revision accepted December 2012

ABSTRACT

Carbonate rocks are heterogeneous at various levels from deposition to diagenesis. Any existing depositional heterogeneity becomes more complex when carbonate rocks are in contact with polar fluids. Our experiments on carbonate rocks show that change in textural heterogeneity leads to heterogeneity in the distribution of storage and flow properties that may govern changes in saturation patterns. This would be akin to any carbonate reservoir with a mix of heterogeneous and homogeneous facies within a formation and their control on saturation distribution in response to a standard imbibition process. Associated with the saturation pattern heterogeneities, the resultant elastic property distributions also change. We quantify this heterogeneity and its effects on flow and seismic properties based on a few textural extremes of fabric heterogeneity in samples that can exist in any typical carbonate reservoir system. Our measurements show that textural heterogeneity can lead to anisotropy in permeability and in acoustic velocities. Permeability anisotropy measurements varied between 40% and 100% while acoustic velocity anisotropy measurements varied between 8% and 30% with lower values for homogeneous samples respectively. Under similar conditions of the saturation experiment (spontaneous imbibition at the benchtop and undrained pressure imbibition at 1000 psi), the imbibing brine replaced 97% of the pore volume in a homogeneous sample (porosity 20% and permeability 2.6 mD) compared to 80% pore volume in a heterogeneous sample (porosity 29% and permeability 23.4 mD). Furthermore, after pressure saturation, a change of +79% in the bulk modulus and -11% in the shear modulus is observed for homogeneous samples in comparison to +34% in the bulk modulus and −1% in the shear modulus for heterogeneous samples, with respect to the dry state moduli values of the samples. We also examined the uncertainties associated with Gassmann models of elastic properties due to variations in fluid saturations.

Our results provide significant information on the saturation and, with it, modulus variations that are often ignored during fluid substitution modelling in time-lapse seismic studies in carbonate reservoirs. We show that the bulk modulus could vary by 45% and the shear modulus by 10% between homogeneous and heterogeneous patches of a reservoir after a water flooding sequence for secondary recovery. Our findings demonstrate the need to incorporate and couple such fabric-controlled saturation heterogeneities in reservoir simulation and in seismic fluid substitution models.

Key words: Heterogeneous, Homogeneous, Carbonates

*Email: ravishar@mymail.mines.edu, ravi4475@gmail.com

INTRODUCTION

Factors such as lithology, texture, saturation amount and distribution and saturant type are known to affect the elastic and flow properties in carbonate rocks (Cadoret, Marion and Zinszer 1995; Knight, Dvorkin and Nur 1998; Adam, Batzle and Brevik 2006). The relation between porosity, pore type and acoustic velocity is well catalogued (for example, Eberli *et al*. 2003). Previous works have debated the importance of porosity and pore fluids on elastic properties of carbonate rocks. For example, Rafavich, Kendall and Todd (1984) and Wilkens, Simmons and Caruso (1984) mentioned that porosity is the most important factor controlling velocity and that the pore-fluid type has no statistical relevance. On the other hand, Assefa, McCann and Sothcott (2003) and Japsen *et al*. (2000) found that pore type, pore-fluid compressibility and saturations are the most important factors controlling elastic properties of carbonate rocks.

The effects of heterogeneity and pore-size distribution in carbonates on transport and elastic properties have largely been neglected. In this study, we investigate how textural heterogeneity might influence flow patterns (Saleh *et al*. 2009) and in turn, the elastic property distributions due to heterogeneous fluid distributions. Such a study assumes significance in assessing the impact of successive production phases or recovery flooding cycles on the textural dependent complexity in saturation patterns and in 4D seismic properties. In particular, we quantify textures (Mukerji and Prasad 2005) and relate them to saturations and elastic property variations. Our study aims to understand the differences in elastic properties of carbonate rocks with heterogeneous and homogeneous textures in response to fluid saturation experiments. Such textural controls on saturation distributions imply that reservoirs with heterogeneous pore distributions might contain complex flow channels. The flow channels, in turn, could lead to saturation changes during a reservoir flooding. Since 4D exploration is used to map saturation changes and bypassed oil, it is important to understand that the preferential flow path may cause heterogeneity in fluid distribution during Enhanced Oil Recovery (EOR) and therefore may impact the resulting reservoir elastic properties. Such information about how flow channels distribute a particular quantity of fluid and how that quantity of fluid will be distributed in a particular facie type is vital to reservoir simulation for improving saturation and bypassed oil maps in heterogeneous reservoirs using time-lapse seismic exploration.

METHODS AND MATERIALS

The samples chosen for our study represent a few examples of fabric heterogeneity that can exist in a typical carbonate reservoir system. Based on comparative textural differences in optical images and through density distribution data and images from CT scans, we termed the samples as 'Heterogeneous', 'Intermediate' and 'Homogeneous' (Fig. 1). The three samples used here were mono-mineralic in composition with 99% calcite (Table 1). These samples were chosen to represent possible extreme members of fabric heterogeneity that might be typical in high-porosity carbonate reservoirs. We carried out petrographic, petrophysical and acoustic investigations on the samples in dry and saturated states. Acoustic velocity and permeability measurements were made along specific planes that marked different propagation directions in each plane. Similar to velocity-porosity correlations, investigations were carried out to find the impact of fabric heterogeneity on the velocity and permeability correlation and the anisotropy in these samples as a probable reason for heterogeneity in saturation and elastic properties.

Petrographic description

A CT scanner and an Environmental Scanning Electron Microscope (ESEM) allowed us to characterize heterogeneity in the carbonate samples, both qualitatively and quantitatively. The CT scanner (Fig. 1) gave us 2D plane images of the samples with resolutions of about 30 micrometres. Low-vacuum ESEM imaging (Fig. 2) and optical microscopic images allowed us to image a detailed microstructure of the samples (Fig. 3). Figure 2 shows ESEM images of the Heterogeneous and Homogeneous samples. The Heterogeneous sample shows poor grain sorting and therefore a wide range of pore-size distribution. The Homogeneous sample on the other hand shows a much more uniform grain size and therefore uniform pore-size distribution. Figure 3 shows optical microscopic images of the Heterogeneous and Homogeneous samples at 25x magnification under plain light. Figure 3(a) shows the disjointed vuggy porosity in the Heterogeneous sample whereas Fig. 3(b) shows a much more uniform porosity distribution in the Homogeneous sample.

Petrophysical description

We employed various methods (volume-weight, Archimidies, Beckman Pycnometer, CMS-300, QEMSCAN, PDPK-200) of

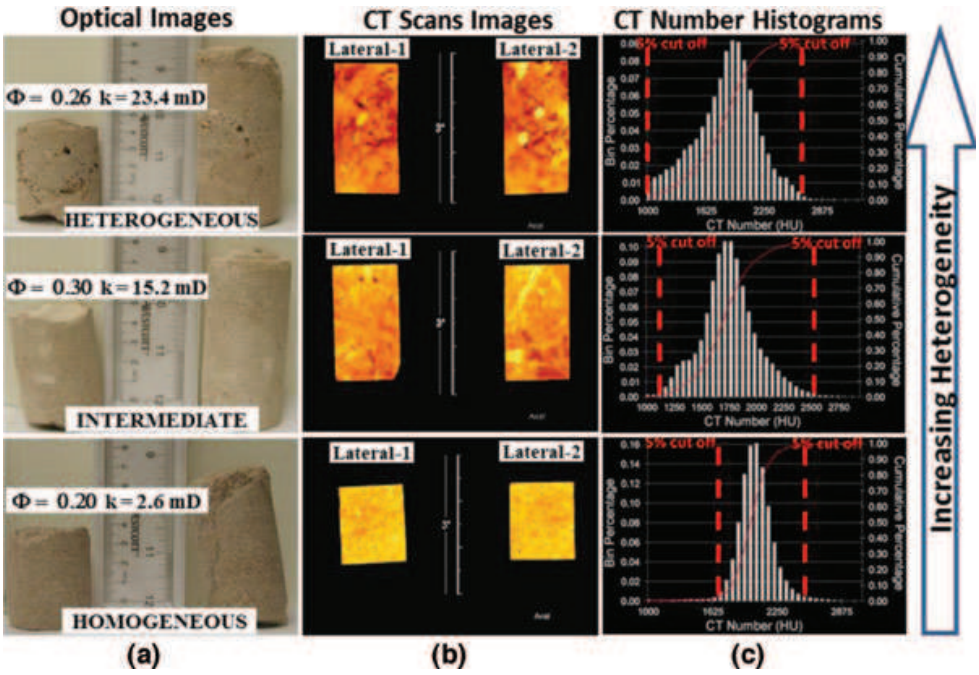

Figure 1 Sample heterogeneity characterization using (a) optical images along with porosity (Φ) and permeability (k) values, (b) CT scan images and (c) CT number distribution. Sample images are arranged with increasing heterogeneity from bottom to top.

Table 1 X-ray diffraction analysis of the Homogeneous, Intermediate and Heterogeneous samples with the weight % distribution of carbonate and non-carbonate minerals.

Sample Textures	Carbonates		Other Minerals		Totals		
	Fe-Calcite	Fe-Dolomite	Quartz	Pyrite	Clays	Carbonates	Other
Heterogeneous	99	Tr	Tr	Tr	1	99	Tr
Intermediate	99	Tr	Tr	Tr	1	99	Tr
Homogeneous	99	Tr	Tr	Tr	1	99	Tr

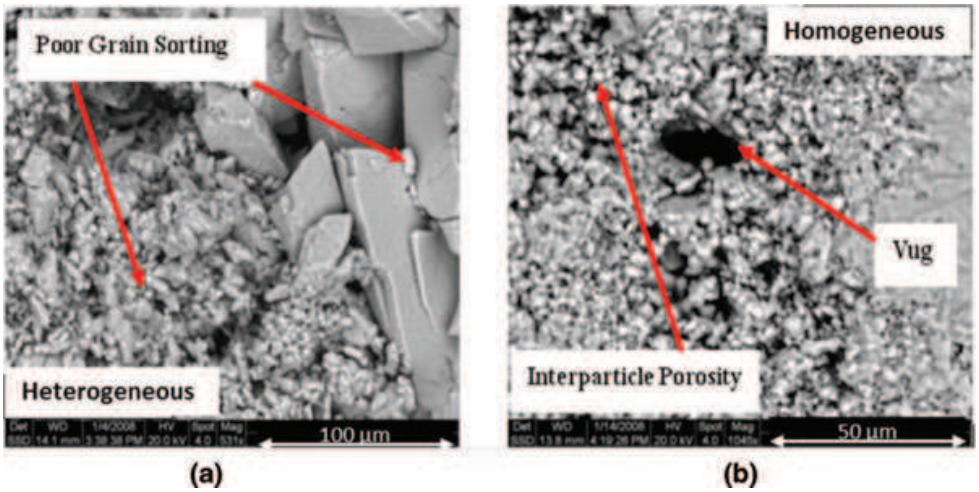

Figure 2 Grain size and qualitative pore-size distribution using an Environmental Scanning Acoustic Microscope (ESEM) in (a) the Heterogeneous sample at 531x and (b) the Homogeneous sample at 1043x.

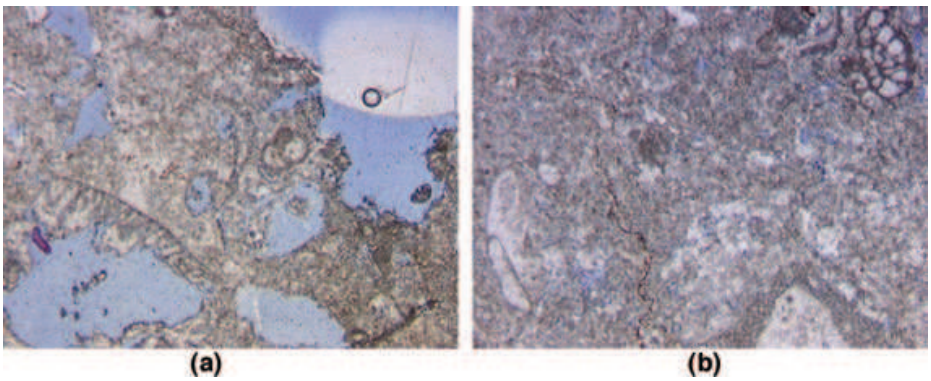

Figure 3 Thin section images at 25x under plain light. (a) Heterogeneous sample and (b) Homogeneous sample.

porosity and permeability measurements and found a good match between the results obtained using different methods. For porosity, the match was within 1–3 porosity units and for permeability the match was between 0.2 mD (Homogeneous sample) to 2 mD (Heterogeneous sample). The porosity and permeability values of the samples used in this work are displayed on the panels in Fig. 1(a).

Textural quantification

The quantification of textural heterogeneity formed a critical link between saturation heterogeneity and elastic property distribution in the samples. We used two different methods to quantify textural heterogeneity in these samples. In the first method, we used equation (1) and Fig. 1(c) panels for each sample to calculate the Heterogeneity Number (HN). We used cut-offs of 5% on the data on both ends of the spread in the Fig. 1(c) panels to avoid errors due to low contribution of the density type to the cumulative bin percentage. We found that the HN for the samples were in accordance with the order of increasing heterogeneity as displayed in Fig. 1.

$$\begin{aligned} &\textit{Heterogeneity Number}\,(\%) \\ &= \frac{\textit{Maximum CT Number}\,(<5\%) - \textit{Minimum CT Number}\,(>5\%)}{2 * \textit{CT Number Highest Bin Percentage}} \\ &\times 100 \end{aligned} \tag{1}$$

where, 'Maximum CT Number (<5%)' is the CT number of the highest value after 5% cut-off

'Minimum CT number (>5%)' is the CT number of the lowest value after 5% cut-off

'CT Number Highest' is the mode of the CT number distribution.

We also used a statistical method (Mukerji and Prasad 2005) to quantify heterogeneity using autocorrelation functions (ACF). Prasad *et al*. (2009) estimated the ACF on organic rich shale (ORS) and showed very distinct ACF signatures in samples with varying textural heterogeneity. Figure 4 from Prasad *et al*. (2009) presents the ACF results in organic rich shale samples along with colour coded textural anisotropy and Correlation Length (CL) calculations. The ACF was

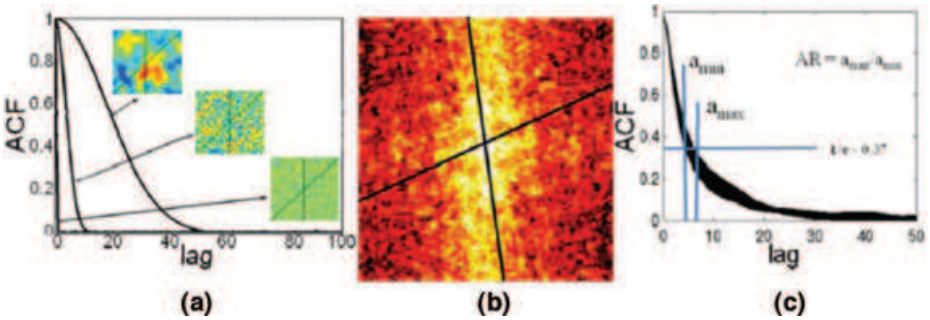

Figure 4 (a) Autocorrelation function (ACF) of the inset images. The image with a coarser texture shows a larger lag value in comparison to the lag value of a finely textured image. (b) Textural anisotropy in a sample in colour code with black lines indicating any two azimuthal directions. (c) The ACF calculated along azimuths from 0–180°. The CL's are picked as lag values of a_{max} and a_{min}. The AR is calculated as the ratio of a_{max} and a_{min}. The figure is from Prasad *et al*. (2009).

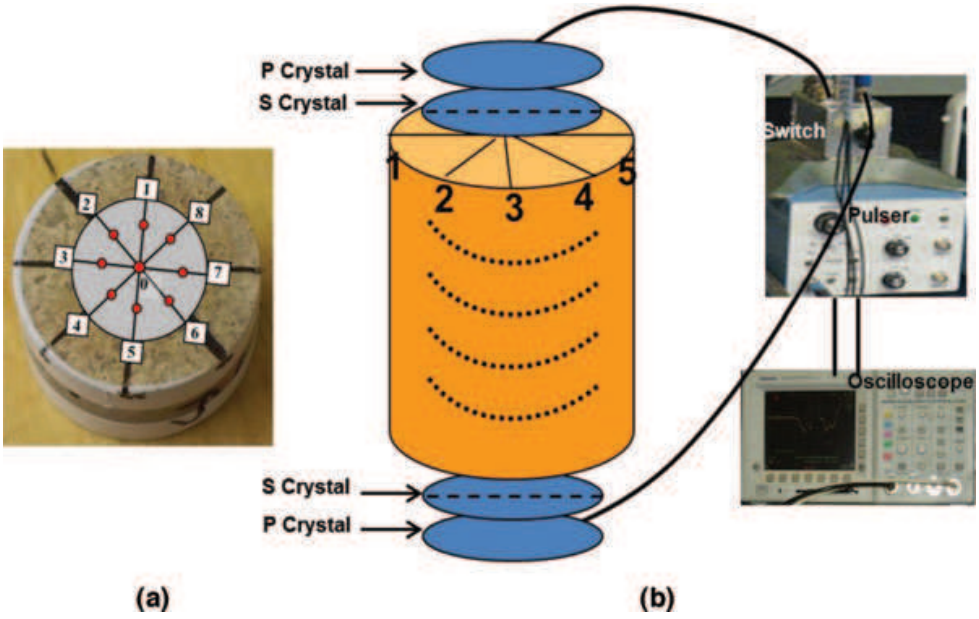

Figure 5 (a) Sample divided into eight equal sections indicated by black solid lines. Shear-wave velocities were measured along the black lines and permeability was measured at each of the red dots and the dots falling along the same lines were averaged to be compared with the shear-wave velocity along that line. (b) Ultrasonic acquisition on samples with P- and S-wave crystals on both ends along with other peripherals. The dotted lines on the sample depict the wave propagation through the sample. The dashed line on the S-wave crystal shows the polarized plane that is matched with the solid black lines on the sample end for measuring velocity along that plane.

calculated in radial profiles along azimuths varying from 0–80°. The CL, which is the value of the lag when the ACF drops to 1/e of its value at zero-lag, was estimated at each azimuth. The ratio of the maximum to minimum CL values was termed as the Anisotropy Ratio (AR).

Acoustic and permeability experiments

We measured the acoustic properties in the samples using the 1 MHz ultrasonic pulse transmission method (Fig. 5). Both the compressive- and shear-wave velocities were measured at ambient laboratory conditions using traveltime observation of the transmitted pulse. Other elastic parameters were derived from the measured velocities using the calculated density in these samples. The acoustic properties in these samples were measured at dry, benchtop saturation and pressure saturation conditions. The samples were marked into eight sections as shown in Fig. 5(a). The sections were designed to measure the impact of fabric heterogeneity on velocity and permeability anisotropy and its control on heterogeneity in saturation and elastic property distribution. As shear waves are plane polarized, indicated by the dashed line in Fig. 5(b), they were acquired along the planes indicated by black solid lines in Fig. 5(a,b). We acquired both the compressive- and shear-wave velocities from point-1 to point-5 (repeat of point-1 for the shear-wave plane). So that the acoustic properties can be related to the permeability, we used a Pressure Decay Profile Permeameter (PDPK-200) to obtain permeability values on the red points as indicated in Fig. 5(a). PDPK-200 is a point permeameter that injects nitrogen gas into the samples using a surface sealing probe. The results from PDPK-200 were highly repeatable under similar acquisition conditions. The permeability values were then averaged between points along a line. The average permeability of the whole sample was obtained by averaging all the PDPK-200 values. Both the velocity and the permeability values were then plotted as a function of sample orientation for analyses on the anisotropic distribution of the velocity and permeability and its impact on heterogeneity in saturation and elastic property distribution.

Saturation experiment

The samples were saturated with 8000 ppm brine in two stages. In the first, the benchtop saturation stage, the samples were saturated under 'Natural (spontaneous) Imbibition' (NIMB) conditions by placing vacuumed dried samples in brine. We weighed the samples to calculate the imbibed brine volumes. In the second, the pressure saturation stage,

the samples were saturated at 1000 psi pressure undrained under 'Forced Imbibition' (FIMB) conditions by gradually increasing pressure in 50 psi steps at a controlled flow rate of 0.5 mL/min up to 1000 psi. After allowing sufficient time for the fluid to reach equilibrium, the samples were reweighed to calculate the additional saturation achieved at this elevated pressure condition. For clarity, a full saturation is considered at 100% fluid saturation. Note that the samples had same lithology and were treated equally to eliminate differences in wettability. Thus, wettability variations can be ruled out as influencing factors for variations in the amount of gas replaced under NIMB and FIMB.

RESULTS

We present the results of our investigations by quantifying the impact of fabric heterogeneity, which is typical of a carbonate system, on heterogeneity in the amount and the pattern of saturation and therefore in elastic property distribution. For time-lapse investigations these observations are very relevant and realistic to be considered in all types of simulation works.

Heterogeneity quantification

In sedimentary rocks, heterogeneity can be compositional or textural. In carbonate rocks, heterogeneity is often also due to post-depositional diagenesis of mineral dissolution and recrystallization that can change the distribution of storage and flow properties as well as rock strength and dynamic elastic properties. The samples used in this study are mono-mineralic (Table 1), from the same formation and come from close by wells, so the textural differences between these samples, as seen in Fig. 1, are considered to arise from diagenesis. The colour contrast in the Fig. 1(b) panels is a reflection of the density variation and could only arise due to different packing of the calcite grains and pore spaces. The petrographic details of these samples are discussed in Figs 2 and 3, which show the ESEM and photo microscope images of the samples.

Table 2 Texture controlled property distribution in the Heterogeneous, Intermediate and Homogeneous samples.

Property	Homogeneous	Intermediate	Heterogeneous
Porosity (%)	20	30	29
Permeability (mD)	2.6	15.1	23.4
Heterogeneity Number (%)	17	34	44
Correlation Length (CL)	3.39	8.3	11.0
Anisotropy Ratio (AR)	1.3	1.3	1.4

In order to quantify the impact of textural heterogeneity on the saturation and elastic properties distribution, we first ascertained the impact of textural heterogeneity on fabric anisotropy and then carried out acoustic and saturation experiments to determine the influence of fabric anisotropy on the heterogeneity of the saturation and elastic properties distribution in the sample.

Textural heterogeneity and fabric anisotropy

Using equation (1) and the panels in Fig. 1(c) we calculated the HN for all three samples. For each sample, the spread of the CT number histogram increases corresponding to the increase in the distribution of colour heterogeneity in the Fig. 1(b) panels and is therefore considered to have a direct bearing on the amount of diagenetic alterations in these samples.

Table 2 presents the results of the ACF calculations and the resulting CL and AR. Figure 6 presents the ACF results in terms of CL in all the azimuthal directions and the resultant AR based on the maximum and minimum correlation lengths. It can be seen from the Fig. 6(ii) panels that textural anisotropy (light blue shade indicated along the black line in the Heterogeneous sample) decreases with a decrease in textural heterogeneity in the samples. For the Homogeneous case in Fig. 6(ii), the directional dependence is almost absent due to more uniformity in the texture distribution in this sample. The Fig. 6(iv) panels show the CL of the samples as a function of lag for different azimuths (0–180°) in terms of the difference between the maximum lag (amax) and the minimum lag (amin) values. These lag values are measured at 1/e of the ACF's maximum value at zero-lag. The lag values are larger for the more heterogeneous sample. The AR is between the maximum and minimum correlation lengths.

A synopsis of the calculated parameters used for quantifying heterogeneity is presented in Table 2. Note that the Heterogeneous and Intermediate samples, which are similar in textural distribution, have more closely related petrophysical properties than the Homogeneous sample that has distant textural as well as petrophysical property values.

The two methods, HN using CT density histograms and AR and CL using ACF, described above for heterogeneity quantification, suggests a positive correlation (Table 2) between independent assessments of the heterogeneity using the

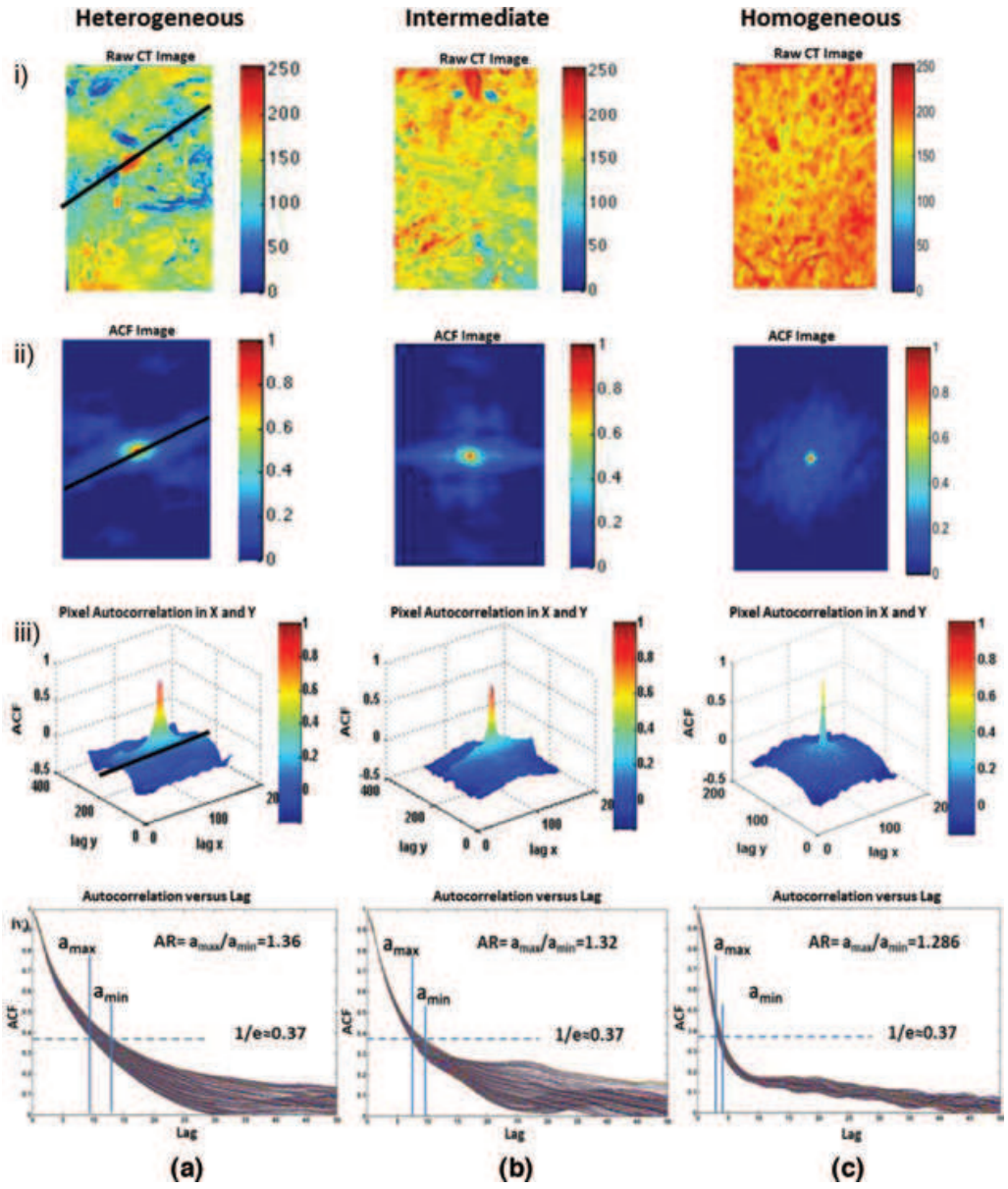

Figure 6 Textural heterogeneity quantification using image autocorrelation of the CT images of the samples. The columns marked (a), (b) and (c) show the analysis for the Heterogeneous, Intermediate and Homogeneous samples, respectively. Each row marked i)–iv) shows the steps in the textural quantification. i) Raw CT images, ii) autocorrelation function (ACF) image of the raw CT image, iii) pixel ACF versus correlation length (CL) in the x and y directions and iv) ACF calculated along azimuths ranging from 0–180°. The correlation length is measured at 1/e of the ACF's maximum value at zero-lag. The AR is between the maximum and minimum correlation lengths.

defined parameters lines HN, CL and AR. Increasing the HN shows an increasing CL and an increasing AR in the samples.

Textural heterogeneity and acoustic anisotropy

Figure 7 shows acoustic characterization of the dry samples. Figure 7(a) shows the CT scan images with the red brace indicating the average resolution size (wavelength size based on the average shear-wave velocity in the dry samples) of the propagating ultrasonic shear wave in each sample. Most of the scattering discontinuities in each sample are close to the size of the wavelength and therefore we assume that the ultrasonic (1 MHz) waveform adequately sampled the visible textural heterogeneity in each of these samples. Care has also been exercised in choosing the size of the crystals to minimize noise in P- and S-wave velocity measurements. The piezocrystals

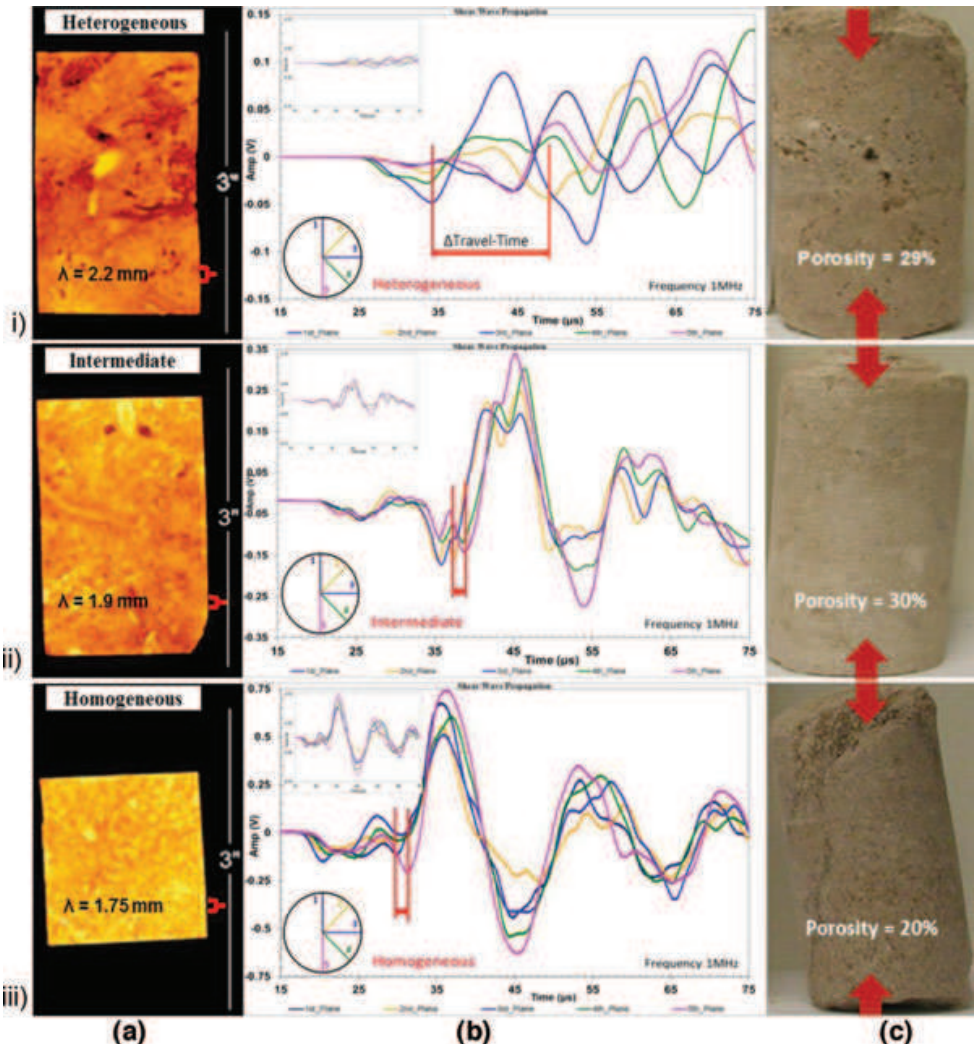

Figure 7 Integrated characterization of the samples using images and shear-wave profiling in the samples. A) CT scan images with sampling resolution of the ultrasonic shear-wavelength (λ) in the three samples. B) Shear-wave profiling in the samples along five different planes around the samples. The main panel is a zoom out of the top-left inset that shows the three samples at equal vertical and horizontal scalings. The three inset panels show the amount of energy loss during shear-wave propagation in these samples. The main panel shows the characteristically different looking shear-wave profiling along the five planes in the three samples. The red vertical bars indicate the maximum difference in the traveltime pick of the shear waves in the five planes and therefore the velocity anisotropy. C) Optical images of the samples showing vugs and solution porosity in the Heterogeneous sample whereas a much more uniform fabric in the Homogeneous sample.

were smaller than sample diameter to avoid excitation waves that would hinder picking the onset time of P- and S-wave signals. At the same time, the crystals were large enough to avoid any ambiguity in terms of measuring phase versus group velocity. Because the original rock was not stratified, the intention was to make group velocity measurements along different planes. The panels in Fig. 7(b) display information on various aspects of the ultrasonic measurements in these samples. The main display of ultrasonic shear-waveform propagation through the samples is a magnified version of the inset display in the top-right corner in these panels. The horizontal scale is the same for both the displays whereas the vertical scale is zoomed out in the main display for ease of traveltime pickup and is different for each sample. The inset display of the waveforms with the same vertical and horizontal scales for each sample shows that the Heterogeneous texture sample causes maximum attenuation of shear-wave energy whereas the Homogeneous texture sample causes the least. Again, in Fig. 7(b) the circular schematic in the lower-left corner shows the shear-wave propagation directions. The vertical red bars indicate the

traveltime difference between the fast and slow ultrasonic shear waves through these samples. Thus velocity anisotropy was caused by the textural heterogeneity in these samples. In the Homogeneous sample, the shear-wave pattern in the five directions showed almost similar behaviour and the shear onset was picked within a narrow traveltime indicating negligible (2%) velocity anisotropy in the sample. On the other hand, in the Heterogeneous sample, the shear-waveform pattern was very different from plane to plane and the shear-wave onset time indicates around 35% velocity anisotropy in the sample. Figure 7(c) shows the optical image of the samples with visible vugs and solution porosity in the Heterogeneous sample and a more uniform fabric in the Homogeneous sample. The red arrows show the direction of the ultrasonic velocity and other rock property measurements in these samples.

Textural heterogeneity and permeability anisotropy

It is common knowledge that porosity and velocity are inversely correlated and that porosity and permeability are directly correlated. By this corollary, it is natural to assume that permeability and velocity will have an inverse correlation to each other. Such correlations would be relatively easy to be observed in clastic sediments where the depositional strata have distinctive lineation to cause velocity (V_{max}, V_{min}) and permeability (k_{max}, k_{min}) anisotropy. However, for carbonate sediments where the deposition is generally of the massive type, existence of such a correlation would be interesting and would help to establish that there could be preferential flow in the samples. Prasad (2003) showed an inverse correlation between velocity and permeability within confines of similar pore geometries. Although the current carbonate samples do not have any lineation in strata, the measurements of permeability and velocity along pre-defined planes (Fig. 5a) show that samples with higher textural heterogeneity have higher permeability and shear-wave velocity anisotropies (Fig. 8a,b). On the other hand, the textural homogeneity observed in the CT images (Fig. 8c) reduces anisotropy in permeability and shear-wave velocity as well. We observe a very strong inverse relation between permeability and shear-wave velocity in the Heterogeneous sample that diminishes to a certain extent in the Intermediate sample and has no such inverse relation in the Homogeneous sample. In the Heterogeneous and Intermediate cases, the permeability values show a sinusoidal pattern. Note that the anomalous high value of permeability in the 3rd orientation of the Homogeneous sample is possibly due to surface inhomogeneity. Similarly, for shear-wave velocity, the Heterogeneous sample shows a strong sinusoidal behaviour that flattens in both the Intermediate and the Homogeneous samples. Based on the azimuthal variation in permeability, it can be expected that the Heterogeneous sample will have more preferential flow of fluids followed by the Intermediate sample and almost negligible in the Homogeneous sample.

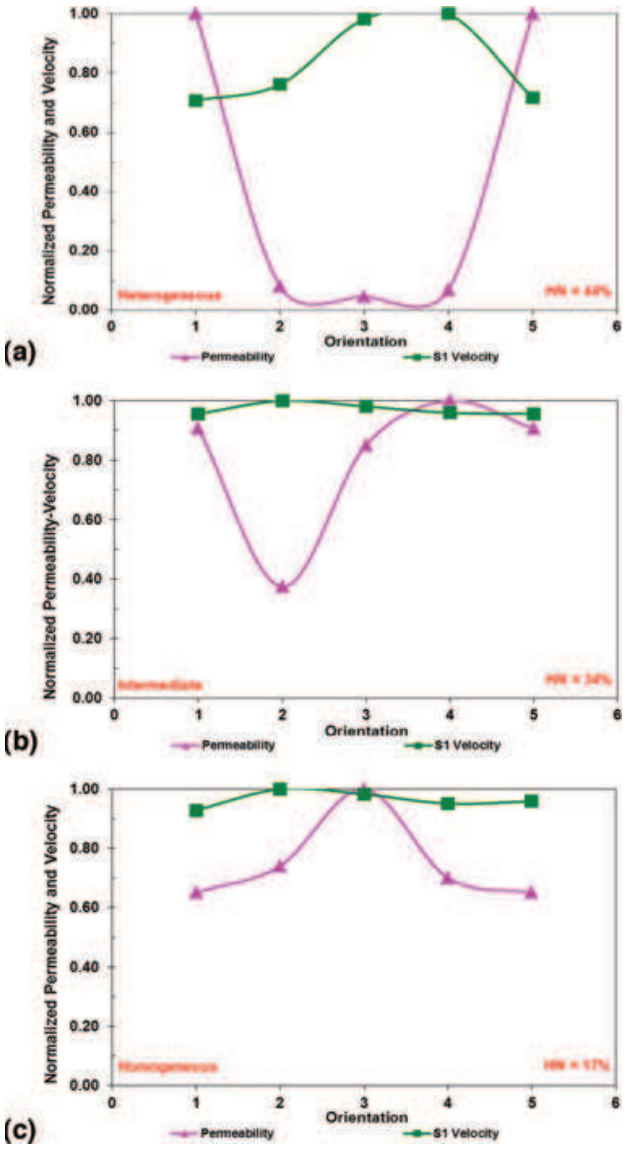

Figure 8 Normalized velocity-permeability anisotropy in the (a) Heterogeneous, (b) Intermediate and (c) Homogeneous samples. The Heterogeneous sample shows maximum anisotropy and the Homogeneous sample shows the least anisotropy in permeability values that were recorded on PDPK-200. Note that in Fig. 9(c), except for orientation 3, the other orientations have very similar values of permeability suggesting that the Homogeneous sample has a very uniform permeability distribution.

Table 3 Measured values of porosity, permeability and brine saturation in the samples at natural and forced imbibition.

Sample	Total Porosity (%)	Permeability (mD)	Natural Imbibition (Sw%)	Forced Imbibition (Sw%)
Heterogeneous	29	23.4	44	80
Intermediate	30	15.2	51	90
Homogeneous	20	2.6	97	99

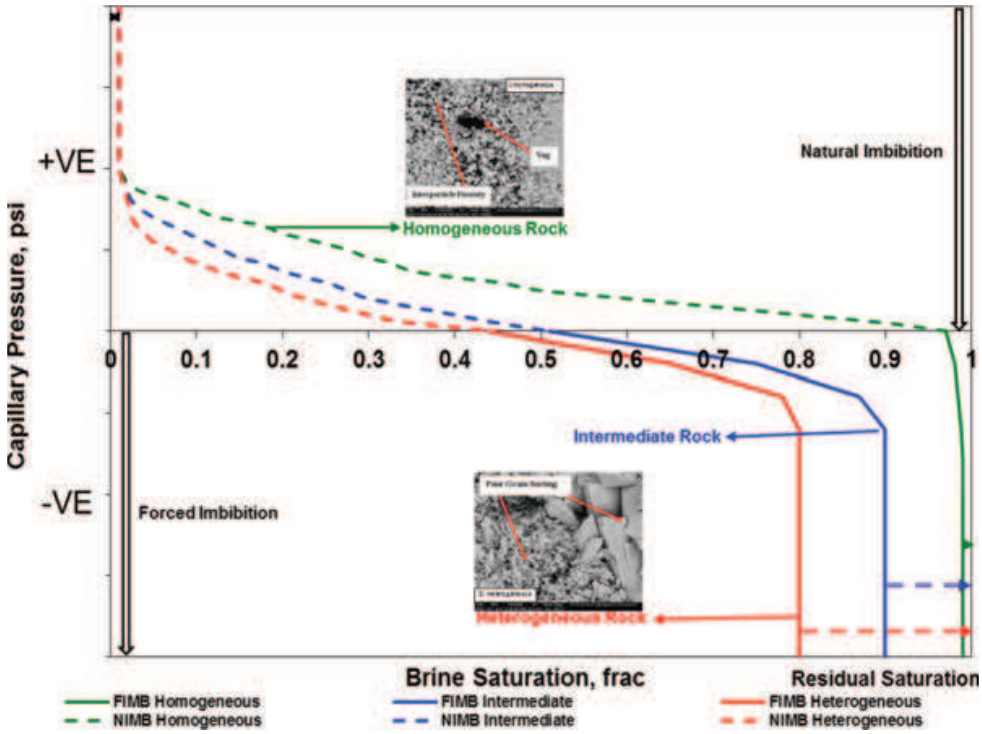

Figure 9 Flow heterogeneity in the samples at partial and end-point saturation values. The colours mark the textural differences with red = Heterogeneous, blue = Intermediate and green = Homogeneous texture. Dashed curves mark the saturation variations with natural imbibition and the solid curves show forced imbibition using vacuum and pressure saturations. Even after forced saturation, the heterogeneous rocks retained 20% residual gas trapped in the sample.

Saturation heterogeneity

We investigated how textural heterogeneity and permeability anisotropy control the amount and pattern of saturation in the samples. This analysis has important implications for assessing successful flooding programs and the likelihood of 4D seismic signatures of patchy flooding success based on large-scale heterogeneities within and between hydraulic units. Although our observations were made on a core-scale, we can expect similar saturation distributions to be repeated on a large, formation scale juxtaposition of textural and heterogeneity variations.

Table 3 presents the porosity, permeability and saturations at NIMB and FIMB conditions. Figure 9 is a graphical presentation of saturation at NIMB and FIMB conditions and shows how the texture of the samples influences the total amount of saturation in these samples under similar saturating conditions. At NIMB conditions, brine invaded 97% of the pore volume in the Homogeneous sample compared to only 44% in the Heterogeneous sample. Furthermore, after FIMB, brine occupied 99% of the pore volume in the homogeneous sample compared to 80% pore volume in the Heterogeneous sample. This difference in saturation signifies that textural heterogeneities within and between hydraulic units might lead to dissimilar hydrocarbon saturations after flooding of a reservoir with a mixed distribution of facies. Significant amounts of gaseous hydrocarbon are likely to remain trapped in heterogeneous formations, up to 20% for the Heterogeneous sample and 10% for the Intermediate sample considered in this work.

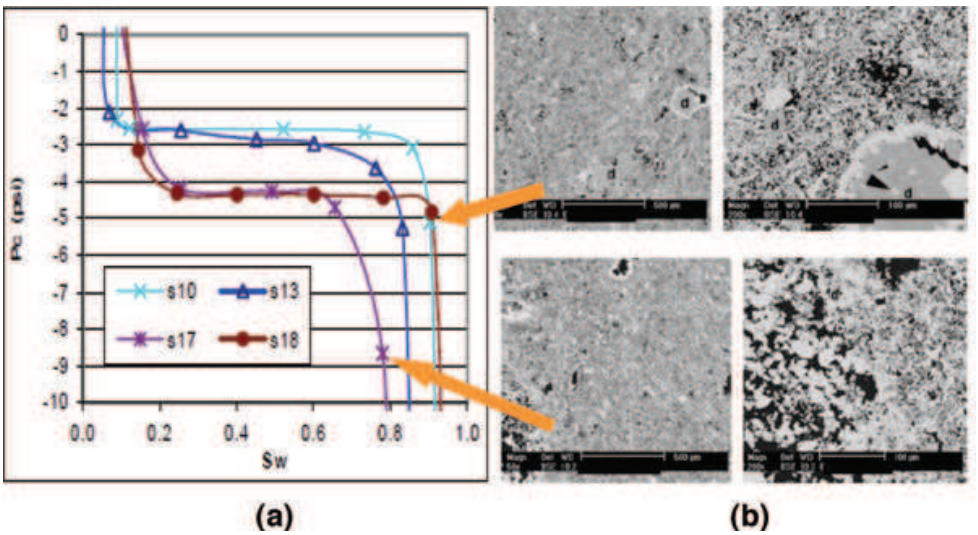

Figure 10 The correlation between capillary pressure curves, saturation and microstructures shows a significant difference in residual water saturation (a). These differences can be compared with textures (b). The Homogeneous samples (#s18 and #s10) show less residual water saturation than the Heterogeneous sample (#s17). All samples have similar porosities between 27–30% (from Masalmeh and Jing 2004).

Special Core Analysis (SCAL) experiments show similar differences in residual saturation based on textures (Masalmeh and Jing 2004). Figure 10 shows imbibition capillary curves and photomicrographs of carbonate samples with similar (27–30%) porosity and similar (2–5 mD) permeability values. The sample (s17) with a very heterogeneous pore-size distribution has more residual water compared to the homogenous sample (s18). This is in good agreement with our results on the Homogeneous and Heterogeneous samples shown in Fig. 9. Despite having higher porosity and correspondingly higher permeability (29%, 23.4 mD respectively) in the Heterogeneous sample, the brine flooding could replace only 80% of the pore volume compared to 99% in the Homogeneous sample with relatively lower porosity and permeability (20%, 2.6 mD respectively).

Saturation effects

We observed in the previous section that heterogeneity in texture can cause heterogeneity in saturation. To determine the impact of heterogeneity in saturation on heterogeneity in elastic properties, we measured the compressional- and shear-wave velocities at each of the pre-defined orientations in the samples as shown in Fig. 4(a). The compressional- and shear-wave velocities in five different orientations for the Heterogeneous, Intermediate and Homogeneous samples are shown in Fig. 11. Each panel displays fifteen measurements, five each for the dry, NIMB and FIMB states. Measurement errors of 2% for the compressive-wave velocity (shown for the dry measurements only) are much less than the observed changes in velocity at the FIMB state and are generally less than the NIMB state except for some cases. The dry velocities show that the Heterogeneous sample, despite having higher porosity (29%), had a stiffer matrix followed by the Intermediate sample (porosity 30%) and then the Homogeneous sample (porosity 20%) that had the softest matrix among the three samples. The measured saturated V_P in the three samples shows that the difference in velocity values between dry to NIMB to FIMB states increases with reduction in the stiffness of the matrix (Fig. 11a). The Homogeneous sample showed an increase (Δ $VP_{FImb.}$) of 415 m/s compared to 167 m/s and 104 m/s increases for the Intermediate and Heterogeneous samples respectively in transition from dry to forced imbibition states.

Similar to the changes in the compressive-wave velocities, the magnitude of the shear-wave velocity differences between the dry and the forced imbibition states increases with reduction in the matrix stiffness (Fig. 12b,d,f). However, compared to the dry state, the saturated Vs is lower suggesting some matrix softening due to saturation. The Homogeneous sample showed a decrease (ΔVS_{FIMB}) of 192 m/s compared to 165 m/s and 136 m/s decreases for the Intermediate and Heterogeneous samples respectively in transition from dry to forced imbibition states. The reduction in shear strength of the sample is minimum for the stiffest (Heterogeneous) matrix sample and maximum for the softest (Homogeneous) matrix sample. Table 4 shows the average values of the compressive- and shear-wave velocities at three different saturations in the samples.

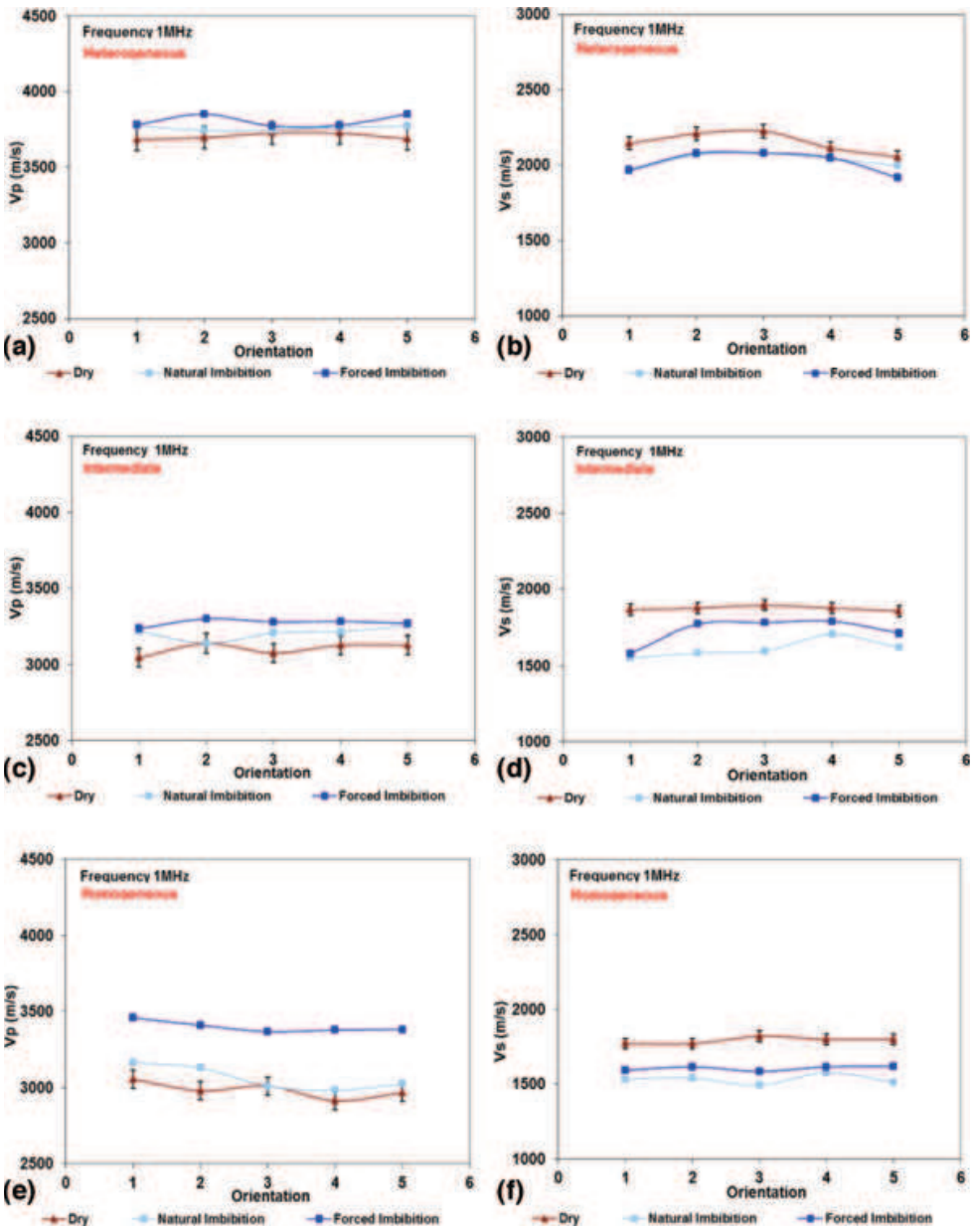

Figure 11 Compressional- and shear-wave velocities respectively for (a) and (b) Heterogeneous sample, (c) and (d) Intermediate sample and (e) and (f) Homogeneous sample. Each panel has fifteen observation points, five each for the dry, natural imbibition and forced imbibition states along the pre-defined five orientations on the samples. The dry observations have error bars for both the velocity (2%) and the modulus (5%) to show that the observation made at the natural and forced imbibition states are above and beyond the error considerations.

DISCUSSION

Saturation effects on the modulus

4D seismic methods are most commonly used to infer saturation variations during the life of a reservoir. Our observation of textural controls on the saturation changes demonstrates the need to incorporate appropriate controls on elastic property changes in a reservoir due to various production schemes. For example, during water flooding in a gas reservoir, presence of homogeneous facies in an heterogeneous formation or vice versa might cause preferential flow of the flooding medium through the homogeneous facie leaving behind amounts of bypassed gas in the heterogeneous facie. Thus, fluid substitution scenarios must incorporate the temporal variations in

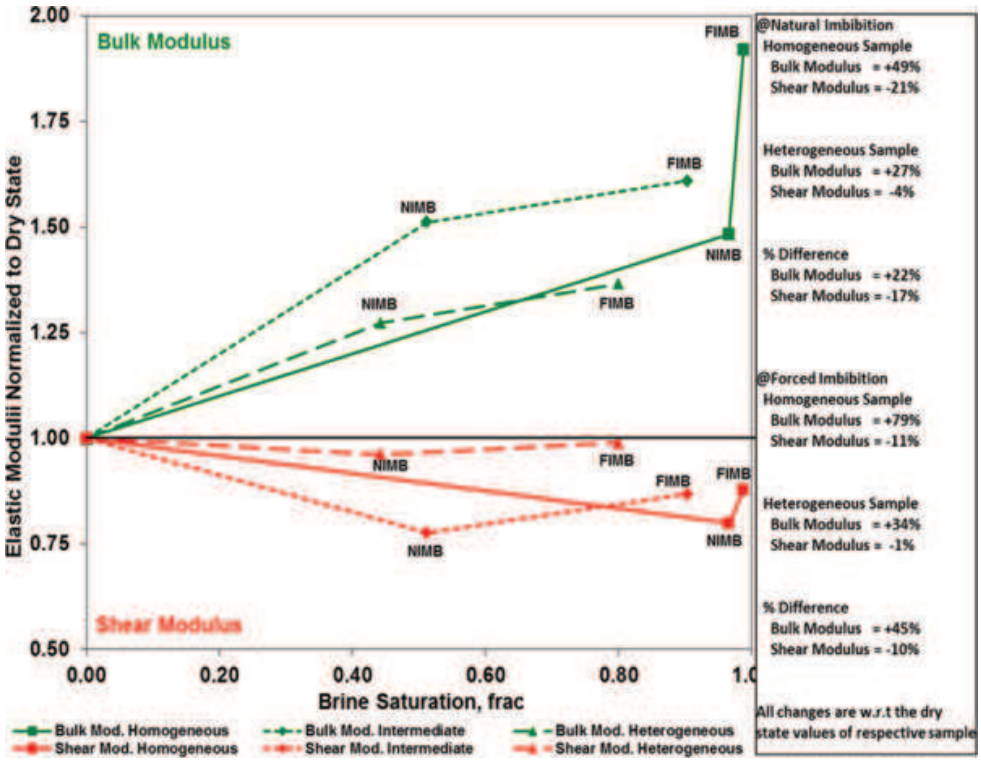

Figure 12 Measured bulk and shear moduli normalized to dry state values. The values are calculated at natural and forced imbibition states using measured compressive- and shear-wave velocity values. The natural and forced imbibition states are indicated for each sample. The summary box on the right-hand side provides details of the change in bulk and shear moduli of the samples in transition from dry to natural imbibition to forced imbibition states.

Table 4 Measured compressive- and shear-wave velocities at the dry, natural imbibition and forced imbibition states.

Sample	Vp at Dry **m/s**	Vp at NIMB **m/s**	Vp at FIMB **m/s**	Vs at Dry **m/s**	Vs at NIMB **m/s**	Vs at FIMB **m/s**
Heterogeneous	3703	3759	3807	2155	2038	2019
Intermediate	3103	3205	3270	1890	1612	1725
Homogeneous	2984	3061	3399	1797	1531	1605

Vp, Vs – compressional- and shear-wave velocities; NIMB, FIMB – natural imbibition (partial saturation), forced imbibition (pressure saturation).

saturations due to spatial variations in textures that may lead to non-uniform saturation in an individual facie type. The following analyses on laboratory experiments with varying brine saturations show potential changes in reservoirs undergoing imbibition during an EOR flooding.

Our natural and forced imbibition experiments showed that the pattern and amount of saturation change seems to be a function of textural heterogeneity. The Heterogeneous sample with 29% porosity shows the least saturation (Sw = 80%) after FIMB. On the other hand, the Intermediate sample, despite having similar (30%) porosity, showed Sw = 90%, while the Homogeneous sample with only 20% porosity shows the maximum saturation (Sw = 99%). Corresponding to these saturation differences, ultrasonic bulk moduli increase and shear moduli decrease (Fig. 12) at partial and pressure saturations compared to the dry state. After pressure saturation, the difference in bulk and shear moduli of the homogeneous and heterogeneous samples was +45% and −10% respectively. In addition to the amount of saturation, the difference in magnitude of the moduli can very well be a function of the pattern of saturation. The X-ray images from Cadoret *et al.* (1995) provided corresponding evidence of patterns of saturation in terms of patchy and uniform gas saturations in carbonates (Fig. 13). This signifies that during EOR schemes, the

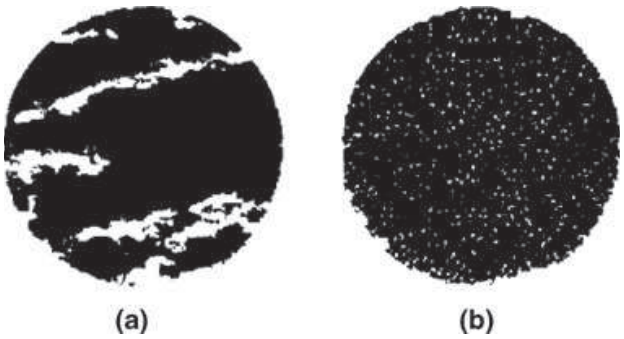

Figure 13 Micrographs of saturation maps of Brauvilliers limestone showing (a) patchy and (b) uniform saturation (Cadoret *et al*. 1995).

reservoir may have texturally controlled saturation patterns that can lead to a heterogeneous elastic property distribution and therefore must be considered for time-lapse seismic investigations.

We investigated two commonly-used models, the Gassmann model (equation (2)) and the Fluid Mixing model (equation (3) from Brie *et al*. 1995) to calculate elastic properties using the rock and fluid saturation information from our experiments. Since the Gassmann model assumes uniform saturation, any deviation between measured and modelled velocities can give us some insight about saturation patterns. The Fluid Mixing model (Brie *et al*. 1995) provides variations in saturation patterns between uniform and patchy to mimic the variations in our samples for spontaneous and forced imbibition. Table 5 presents the list of constants (Mavko, Mukerji and Dvorkin 2009) used in our calculations.

$$K_{sat} = K_{dry} + \frac{\left(1 - \frac{K_{dry}}{K_{solid}}\right)^2}{\left(\frac{\Phi}{K_{fl}} + \frac{(1-\Phi)}{K_{solid}} - \frac{K_{dry}}{K_{solid}^2}\right)}, \quad (2)$$

where, K_{sat} is the saturated bulk modulus

K_{dry} is the dry rock bulk modulus

K_{solid} is the mineral bulk modulus

K_{fl} is the fluid bulk modulus (Reuss fluid)

Φ is the porosity of the rock

$$K_{fluid} = (K_{liquid} - K_{gas}).(1 - S_{gas})^e + K_{gas}, \quad (3)$$

where, K_{fluid} is the bulk modulus of the fluid mixture

K_{liquid} is the bulk modulus of the liquid component in the formation

K_{gas} is the gas bulk modulus

S_{gas} is the saturation of gas

Table 5 List of constants used in the calculation of the modelling parameters (from 'Handbook of Rock Physics' by Mavko *et al*. 2008)

Property/ Mineral	Bulk Modulus GPa	Shear Modulus GPa	Density kg/m^3
Calcite	75	31	2710
Clay	21	7	2600
Brine	2.5	0	1100
Air	0.000147	0	1.25

e describes the mixing of the fluids and ranges from 1–40: e = 1 implies that the fluids are mixed in series whereas e = 40 is used for mixing fluids in parallel.

Figure 14 shows the measured and modelled velocities as functions of saturation. As shown earlier (Winkler 1986; Eberli *et al*. 2003; Assefa *et al*. 2003), the Gassmann model underpredicts measured velocity values for the Heterogeneous and Intermediate texture samples. For the Homogeneous sample, the Gassmann model prediction is about the same as the measured values indicating homogeneous saturation. The Fluid Mixing model approaches the measured bulk moduli only for e = 1 in the heterogeneous and intermediate samples indicating extreme patchiness in saturation. The mismatch between the ultrasonic velocity data and the Gassmann model in saturated carbonates is due to two main reasons: 1) partial and patchy saturations are prevalent in carbonate rocks, whereas the Gassmann model is valid for uniform saturations (Sengupta and Mavko 2003) and 2) frequency dispersion or local flow mechanisms may influence measured velocities whereas the Gassmann model is a low-frequency approximation (Mavko and Jizba 1991). The difference between the Gassmann low-frequency approximation and Biot's high-frequency approximation was shown to be minimal when compared with the measured ultrasonic velocity (Fabricius Bächle and Eberli 2010). We therefore infer that patchiness in saturation due to textural heterogeneity is the dominant factor controlling velocities compared to the local flow mechanism.

The HN's for the heterogeneous and intermediate samples were comparable (44% and 37%, respectively) compared to 17% textural heterogeneity for the homogeneous sample. Figure 14 also shows that both porosity and K_{dry} influence fluid substitution. Elastic property variations upon saturation are less when K_{dry} is high. For example, the heterogeneous and intermediate samples have similar porosity. However, since the intermediate sample has lower K_{dry}, it has a larger variation in K_{sat}.

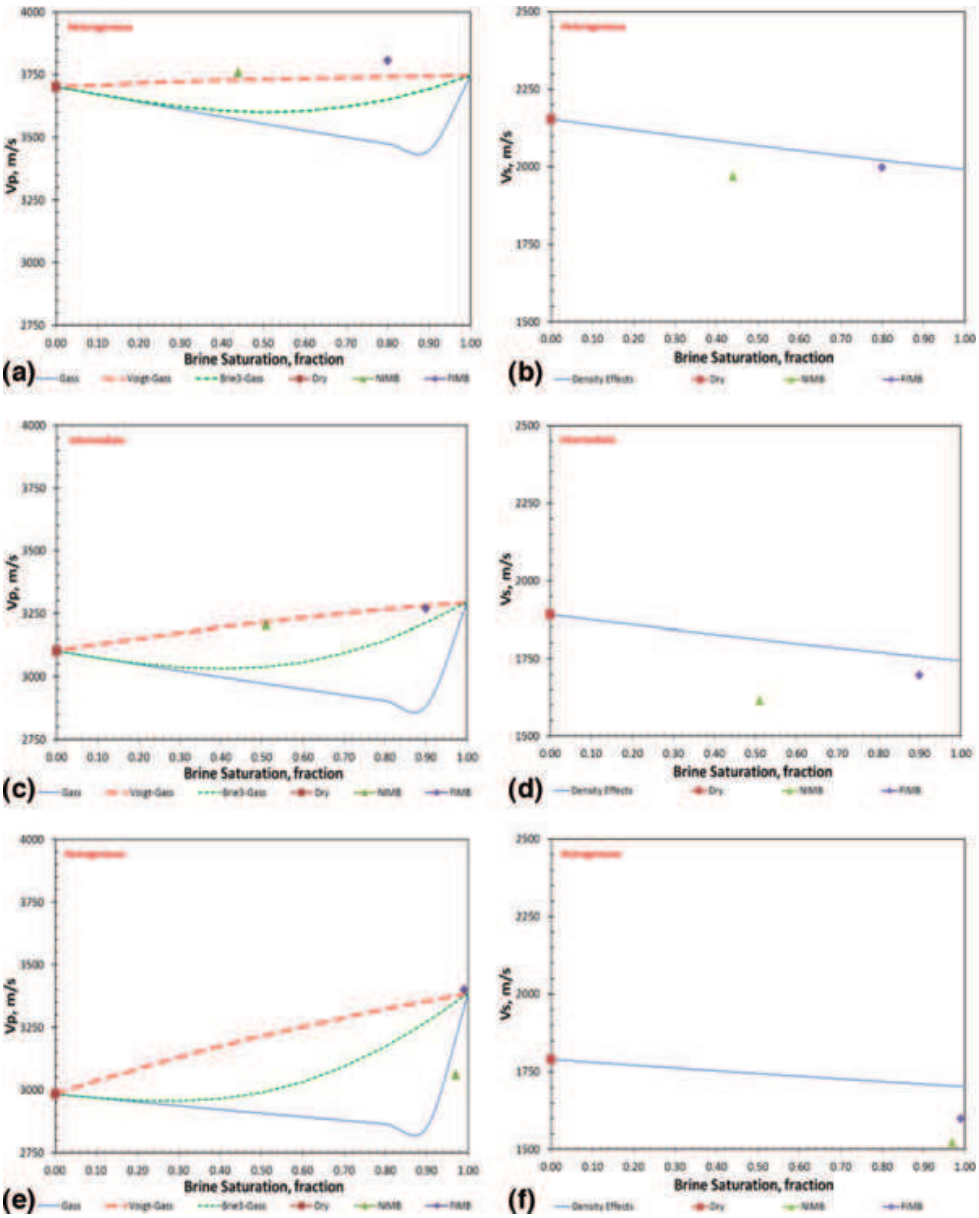

Figure 14 Measured and modelled (a) Vp and (b) Vs as a function of brine saturation in the Heterogeneous sample, (c) and (d) for the Intermediate sample and (e) and (f) for the Homogeneous sample. For Vp in (a), (c) and (e) we used the Gassmann and Fluid Mixing models (Brie *et al*. 1995). The Gassmann model is represented by the solid blue line, the Fluid Mixing model by dashed lines with the red dashed line representing a patchy mixing of fluids (e = 1) and the green dashed line representing the power law mixing of fluids (e = 3).

We also found that the saturation in these samples has affected the shear strength of the samples (Fig. 14b,d,f). The modelled V_S values presented in the bold blue line incorporate the fluid density effects in combination with the dry state shear modulus of the samples. At the FIMB state, the rigidity of the homogeneous rock with the softest of the rock frames is most affected by the saturation whereas in the heterogeneous rock with the stiffest of the rock frames, the saturation has a smaller effect on the shear strength of the rock. The reasons for such a reduction in shear strength upon saturation have been detailed in Khazanehdari and Sothcott (2003). The most common of them is the changes in surface energy due to fluid-solid interactions (Tutuncu *et al*. 1998) or reduction in activation energy due to weakening of solid-solid

bonds (Martin 1972). The fluid-solid interactions responsible for weakening the shear strength occurs for the reasons that in most of the cases the imbibed fluid is not similar to the formation fluid and hence is not in equilibrium with the host rock as the original formation water would be. In reactive rocks like carbonates, such a difference in the salinity of the imbibed fluid will more readily initiate geochemical reactions between the host rock and the imbibed fluid. Similar was the difference in the salinity of the imbibed (8000 PPM-Low Salinity Brine) fluid and the original formation (60 000 PPM) fluid that could easily become a potential reason for initiating a geochemical reaction responsible for weakening solid-solid bonds and thus the shear strength of the rocks. Also our results show that a weaker rock frame (homogeneous rock) will have more shear weakening effects than a stiffer rock frame (heterogeneous rock) when treated with a similar salinity fluid. This weakening in shear strength has a greater time-lapse implication for geomechanical applications in these reservoirs.

Our results have implications for reservoir characterization in carbonate formations that involve integration of various data types such as petrophysical, rock physics and seismic data, as well as reservoir simulations to obtain realistic flow and elastic property variations with time. Often analogues and models are used to predict reservoir properties and changes therein due to production or secondary recovery processes. However, although saturations might be uniform in the initial phase of a reservoir development, textural heterogeneity and resulting anisotropy can lead to patchy depletion during production or during flooding treatments. These changes can be either masked or accentuated in 4D seismic maps and potentially lead to errors in estimates of bypassed zones.

Heterogeneity effects on saturation and the modulus

Heterogeneity in fabric can cause heterogeneity in the distribution of flow properties and therefore can influence distribution of saturation in the rock. The saturation itself can influence the overall elastic effects in place depending upon the types (uniform, patchy) of saturation in a facie type as shown in Fig. 12. Table 6 presents a synopsis of the heterogeneity effects on saturation and the resulting modulus as measured in the present work. This table shows that the Heterogeneous and Intermediate samples, which are close to each other in textural distribution of grains and pores, have a more similar distribution of the texture related properties like the petrophysical properties and textural anisotropy. Whereas, the Intermediate and Homogeneous samples, despite having a large difference in petro- physical property values, have very similar acoustic properties in both the dry and fluid saturated cases. Since acoustic properties are more of a function of the stress propagation matrix, these two samples having a similar stiffness matrix is the most plausible explanation for similar acoustic behaviour in these samples.

Table 6 Effects of textural heterogeneity on saturation and the elastic modulus in the samples

Texture/ Property	Homogeneous	Intermediate	Heterogeneous
Porosity (%)	20	30	29
Permeability (mD)	2.6	15.2	23.4
Heterogeneity Number (%)	17	34	44
Residual Saturation (%)	1	10	20
K dry (GPa)	9.96	9.19	14.4
G dry (GPa)	6.88	6.75	8.7
K sat (GPa)	19.01	14.77	19.56
G sat (GPa)	5.95	6.18	8.5
K Gassmann (GPa)	10.20	9.20	14.41
ΔK (Sat.-Dry) GPa	9.05	5.58	5.16
ΔG (Sat.-Dry) GPa	−0.93	−0.57	−0.2

CONCLUSION

The two most challenging and unresolved parameters to influence enhanced recovery in carbonate reservoirs are 'heterogeneity in texture' and 'heterogeneity in saturation'. Our study has provided an understanding about the influence of heterogeneity in fabric and saturation on the seismic rock properties. We have shown that

1. Textural heterogeneity leads to differences in residual gas saturation that potentially can be smaller under pressure saturation (FIMB) schemes in analogy to enhanced flooding scenarios.
2. The difference in residual gas saturation cause significant difference in elastic properties as compared to dry state values. Thus, in addition to porosity, amount and pattern of saturation within that porosity will also change effective elastic properties of the rocks. Understanding such interrelations can be critical when analyzing time-lapse elastic property changes in a reservoir under EOR treatments.

3. Shear modulus was sensitive to changes in saturation: brine saturation caused significant weakening of the shear modulus. Assuming constant shear modulus can have serious implications in stability analysis of reservoir during enhanced recovery flooding and also for evaluating time-lapse seismic response.
4. The Gassmann model can reliably be used to predict seismic velocities in homogeneous rocks. Heterogeneous rocks however, develop patchy saturation. Here, the Gassmann model of uniform saturation is not sufficient to predict 4D saturation changes; the Brie fluid mixing can reduce uncertainty in predicting seismic velocities.

ACKNOWLEDGEMENT

We express our sincere thanks to the Petroleum Institute, Abu Dhabi, OCLASSH and the DHI/Fluids consortium for financial support. We also thank members of the Center for Rock Abuse at CSM for valuable technical discussions.

REFERENCES

Adam L., Batzle M. and Brevik I. 2006. Gassmann's Fluid Substitution and Shear Modulus Variability in Carbonates at Laboratory Seismic and Ultrasonic Frequencies. *Geophysics* **71**, F173–F183.

Assefa S., McCann C. and Sothcott J. 2003. Velocities of Compressional and Shear Waves in Limestones. *Geophysical Prospecting* **51**, 1–13.

Brie A., Pampuri F., Marsala A.F. and Meazza O. 1995. Shear-Sonic Interpretations in Gas-Bearing Sands. SPE ATCE, SPE 30595, 701–710.

Cadoret T., Marion D. and Zinszner B. 1995. Influence of frequency and fluid distribution on elastic wave velocities in partially saturated limestones. *Journal of Geophysical Research* **100**(B6), 9789–9803.

Eberli G.P., Baechle G.T., Anselmetti F.S. and Incze M.L. 2003. Factors Controlling Elastic Properties in Carbonate Sediments and Rocks. *The Leading Edge* 654–660.

Fabricius I.L., Bächle T.G. and Eberli G.P. 2010. Elastic Moduli of Dry and Water-Saturated Carbonates – Effect of Depositional Texture, Porosity and Permeability. *Geophysics* **75**(3), 65–78.

Gassmann F. 1951. Über die Elastizität poröser Medien. *Vierteljahresschrift der Naturforschenden Gesellschaft in Zurich* **96**, 1–23.

Japsen P., Wagner H., Gommesen L. and Mavko G. 2000. Rock Physics of Chalk: Modeling the Sonic Velocity of the Tor Formation, Danish North Sea. EAGE 62nd Conference and Technical Exhibition.

Khazanehdari J. and Sothcott J. 2003. Variation in dynamic elastic shear modulus of sandstone upon fluid saturation and substitution. *Geophysics* **68**, 472–481.

Knight R., Dvorkin J. and Nur A. 1998. Acoustic Signatures of Partial Saturation. *Geophysics* **63**(1), 132–138.

Martin R.J. 1972. Time-Dependent Crack Growth in Quartz and Its Application to the Creep of Rocks. *Journal of Geophysical Research* **77**, 1406–1419.

Masalmeh, S. K. and Jing, X. D. I. 2004. Carbonate SCAL: Characterisation of Carbonate Rock Types for Determination of Saturation Functions and Residual Oil Saturations. In: International Symposium of the Society of Core Analysts, Abu Dhabi, UAE.

Mavko G. and Jizba D. 1991. *Estimating Grain-Scale Fluid Effects on Velocity Dispersion in Rocks Geophysics*. Volume: 56 Issue: 12, pp. 1940–1949.

Mavko G., Mukerji T. and Dvorkin J. 2009. *The Rock Physics Handbook*. Cambridge University Press, April 2009.

Mukerji T. and Prasad M. 2005. Image processing of acoustic microscopy data to estimate textural scales and anisotropy in shales. In: *Acoustical Imaging*, Vol. 28 (ed. A.P. Michael), pp. 409–416. Springer Verlag.

Prasad M. 2003. Correlating Permeability with Velocity using Flow Zone Indicators. *Geophysics* **68**, 108–117.

Prasad M., Mukerji T., Reinstaedtler M. and Walter A. 2009. Acoustic Signatures, Impedance Microstructure, Textural Scales, and Anisotropy of Kerogen-Rich Shale. SPE 124840, SPE, ATCE 09, Louisiana.

Rafavich F., Kendall C. and Todd T. 1984. Relation between the Acoustic Properties and the Petrographic Character of Carbonate Rocks. *Geophysics* **49**, 1622–1636.

Saleh M., Vega S., Prasad M. and Sharma R. 2009. A Study of Permeability and Velocity Anisotropy in Carbonates. Research and Development Forum, SEG, Bahrain.

Sengupta M. and Mavko G. 2003. Impact of flow-simulation parameters on saturation scales and seismic velocity. *Geophysics* **68**, 1267–1280.

Tutuncu A.N., Podio A.L., Gregory A.R. and Sharam M.M. 1998. Non-linear viscoelastic behaviour of sedimentary rocks. Part I: Effect of frequency and strain amplitude. *Geophysics* **63**, 184–194.

Wilkens R., Simmons G. and Caruso L. 1984. The Ratio V_P/V_S as a Discriminant of Composition for Siliceous Limestones. *Geophysics* **49**, 1850–1860.

Winkler K. 1986. Estimates of Velocity Dispersion between Seismic and Ultrasonic Frequencies. *Geophysics* **51**, 183–189.